
Invariant Information Distillation for Unsupervised Image Segmentation and Clustering

Xu Ji
University of Oxford
xuji@robots.ox.ac.uk

João F. Henriques
University of Oxford
joao@robots.ox.ac.uk

Andrea Vedaldi
University of Oxford
vedaldi@robots.ox.ac.uk

Abstract

We present a new method that learns to segment and cluster images without labels of any kind. A simple loss based on information theory is used to extract meaningful representations directly from raw images. This is achieved by maximising mutual information of images known to be related by spatial proximity or randomized transformations, which distills their shared abstract content. Unlike much of the work in unsupervised deep learning, our learned function outputs segmentation heatmaps and discrete classifications labels directly, rather than embeddings that need further processing to be usable. The loss can be formulated as a convolution, making it the first end-to-end unsupervised learning method that learns densely and efficiently for semantic segmentation. Implemented using realistic settings on generic deep neural network architectures, our method attains superior performance on COCO-Stuff and ISPRS-Potsdam for segmentation and STL for clustering, beating state-of-the-art baselines.

1 Introduction

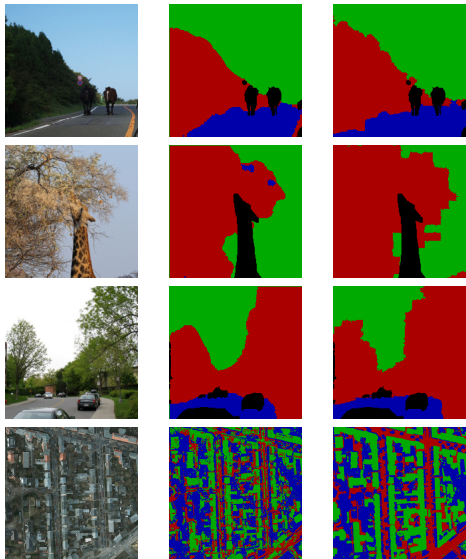
Modern deep learning methods have demonstrated remarkable success in image understanding tasks such as segmentation, classification and detection (Girshick et al. [2014], Long et al. [2015], Simonyan and Zisserman [2014]). However, the most successful methods are heavily dependent on fully supervised learning. The need for very large quantities of labeled training data severely limits their applicability to many cases of interest. Solving this requires developing learning principles that do not require expensive data annotation, which been the focus of recent research efforts supported by different interpretations of what it means to find structure in raw data (Pathak et al. [2016], Noroozi and Favaro [2016], Lee et al. [2017], Chang et al. [2017]).

The need for unsupervised learning is particularly great for image segmentation, where the labelling effort required is especially expensive. Despite this, unsupervised semantic segmentation remains relatively unexplored (Greff et al. [2016] demonstrated some potential for instance segmentation). While one could argue that any unsupervised image clustering technique can be applied to segmentation by treating patches as images, this is not necessarily practical (a single 200×200 image has 40000 patches), inspiring the question of whether an unsupervised method can be designed to be dense and efficient from the outset. Additionally, there is potential to leverage the denseness of the segmentation problem - for example by using extra information in the spatial relations between patches - to outperform adapted image classification methods that act on patches in isolation.

We present a simple new approach to unsupervised image understanding called *Invariant Information Distillation* (IID). Given only an unstructured collection of images as input, IID learns to map images or pixels directly to classes representative of their abstract visual content. The key idea is to induce a representation by seeking what is in common between two different images known to share the same visual phenomenon whilst discarding image-specific details, which allows for deeper abstraction than if they were pairs of identical images. We show that this can be elegantly formulated

as maximizing mutual information under a bottleneck restraint. Since the setting is unsupervised and associations between images are unknown, image pairs can be generated using image transformations, and in the case of segmentation, from known spatial proximity. The use of transformations and patch proximity has the effect of encouraging learned classes to be invariant to geometric and color nuisance transformations. Crucially, maximising mutual information between the predictions of spatially proximal patches for segmentation can be formulated as a convolution, allowing for efficient and straightforward implementation with any deep learning library.

Our contributions can be summarized as follows. We formalize the concept of mutual information distillation and use it to define a differentiable loss layer that can be used in backpropagation (Section 3.1). We apply distillation to learning invariance to transformations, obtaining a method for unsupervised image clustering (Section 3.2), and invariance to local spatial shifting of image patches, used for unsupervised semantic segmentation (Section 3.3). We formulate the latter as convolution and show that our method has several theoretical and practical benefits, including properties of invariance to noise, contextual informativeness, smoothing, and controllable cluster mass equalization, whilst maintaining a simple objective function without any separate terms or weighting factors. We also explicitly relate information distillation to other clustering principles (Section 3.4). For the main application of segmentation we achieve 71.1% accuracy on COCO-Stuff-3 (Caesar et al. [2016]) compared to top baseline 61.8% and 72.5% on Potsdam-3 (ISPRS) compared to top baseline 55.5%. We also demonstrate competitive results for image classification, attaining 33.8% on unlabelled STL-10 (Coates et al. [2011]) compared to top baseline 32.3%.



(a) Segmenting COCO-Stuff and Potsdam. Left to right: original image, IID predictions, ground truth.



(b) Classifying STL. Top to bottom: projections of random network predictions and IID predictions.

2 Related work

Methods for learning with reduced manual supervision can be separated into two main camps. The first comprises *semi*-supervised methods that use partially labelled datasets (Papandreou et al. [2015]). These methods resemble fully-supervised learning in that one has access to labels corresponding to the target task. The other camp comprises methods that learn using *self*-supervised generative or auxiliary tasks, such as autoencoder image reconstruction (Vincent et al. [2010]), inpainting (Pathak et al. [2016]), solving jigsaw puzzles (Noroozi and Favaro [2016]), spatial-temporal order prediction (Lee et al. [2017], Cruz et al. [2017], Doersch et al. [2015]), predicting egomotion (Agrawal et al. [2015]), or learn from repurposed datasets such as segmentation from image-level labels (Pathak et al. [2015]) or bounding boxes (Hu et al. [2017], Dai et al. [2015]). A disadvantage of these methods is that they either require surrogate labels in the form of separate modalities or necessitate a two-step approach: features are first learned using a proxy task, and then must be post-processed to be of use, typically either with a fully supervised last stage, or a separate spectral or k-means clusterer.

Learning from adjacent image patches. One variant of our method learns from adjacent image patches. This is similar to the approach of Isola et al. [2015], who predict whether two patches are adjacent or not. Like the other proxy task methods discussed above, this approach can learn a data representation, but cannot directly perform image segmentation and clustering as we do.

Deep clustering. Our approach can also be seen as a clustering method, most of which are unsupervised. There is of course a very significant amount of literature on clustering, so we only cite a few recent methods that are most relevant to our work. Chang et al. [2017] (DAC) uses a randomly-initialized network to embed data in a vector space and then gradually modifies it to let the embeddings form well separated clusters. The outcome depends strongly on the initialization and learning schedule. Since the embedding vectors look like indicator vectors of clusters, this is one of the few approaches that, like ours, directly trains a deep neural network to output cluster identities. A related method, Xie et al. [2016] (DEC), learns embeddings that are fed to an external clustering mechanism, reminiscent of k-means. Yang et al. [2016] is similar to both in the sense that it relies on disentangling properties (Greff et al. [2015]) already present in a randomly initialised CNN to produce an over-clustering, which is then iteratively refined using agglomerative clustering.

Learning from denoising images. Greff et al. [2016] is a generative approach; a function is trained to denoise its input using several clusters to distribute the representation. Different instances of the same visual phenomenon are separated, whereas we aim to group such instances together. However, since the objective is to reconstruct the original image based on features of a noisy copy, it uses the same concept of learning a representation that persists through visual distortion.

Co-learning. The idea of learning a data representation from related observations is not new. An early work that resembles ours is Becker and Hinton [1992]. They maximise agreement between representations of 2D images to learn depth, using an objective corresponding to maximising mutual information between the input and the average of the data representations. Co-learning has also been explored in the context of clustering by co-clustering methods, dating back to the pioneering work of Hartigan [1972]. Many information-theoretic variant of such approaches have been proposed, as discussed by Wang et al. [2010]. The latter are generally related to the information bottleneck principle (Friedman et al. [2001]).

More recently Dosovitskiy et al. [2016] explored using invariance to image transformations for feature learning, by taking multiple transforms per image and treating each of these sets as a class. However, being an instance based approach requiring one class per patch per image, scaling to segmentation is difficult due to significant memory complexity and consequent reduction in batch size (see Section 4.2). In contrast, IID’s ability to densely exploit spatial proximity and efficient formulation as a convolution makes it ideal for segmentation. Note also the fundamental premise of IID quite different; our approach builds on the analysis of proximal or related patches, which in general cannot be obtained as a transformation of another patch (for example because their domain is disjoint). Dosovitskiy does not consider spatial proximity at all, but only global image transformations with the same domain, and therefore the similarity to IID is manifest only in the special case of image clustering, not segmentation. Even in this case, there are significant differences, notably our use of information theory to enable mass equalised clustering, and end-to-end formulation with the clusters being part of the network model whereas Dosovitskiy requires an external feature clustering phase.

3 Invariant Information Distillation

This section introduces our key contribution, Invariant Information Distillation (IID), starting from the concept of Information Distillation (ID) (Section 3.1), extending it to unsupervised image clustering and segmentation by incorporating invariance to transformations (Sections 3.2 and 3.3), and finally relating it to popular clustering principles (Section 3.4).

3.1 Information Distillation

Our goal is to learn to associate with each image \mathbf{x} a label $\Phi(\mathbf{x})$ that is representative of its visual content, without any ground truth for direction. To achieve this, consider the related problem of *co-distillation*; assume we have two observations \mathbf{x} and \mathbf{y} of the same underlying phenomenon, and seek a function Φ that captures what is in common between them. Formally, it is natural to cast the

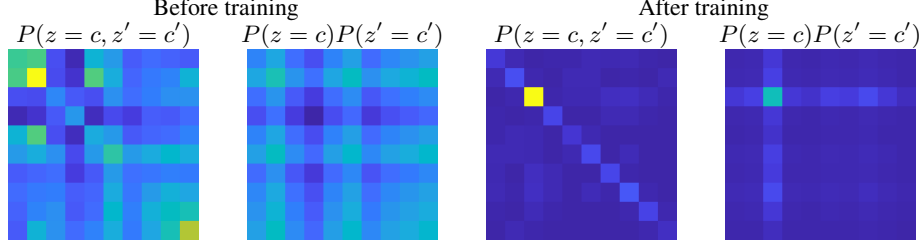


Figure 2: Joint probability and product of marginal probabilities of 10 clusters, measured both before and after training. Cluster z is indexed along the rows, and z' along the columns; brighter values indicate higher probability. Our mutual information objective (eq. Eq. (2)) can be interpreted as maximising the KL-divergence between the joint probabilities (left) and product of marginals (right).

latter as the problem of learning to maximize the information between their representations:

$$\max_{\Phi} I(\Phi(\mathbf{x}), \Phi(\mathbf{y})). \quad (1)$$

However, due to the data processing inequality $I(\mathbf{x}, \mathbf{y}) \geq I(\Phi(\mathbf{x}), \Phi(\mathbf{y}))$ (Cover and Thomas [2012]), we see that this is trivially solved by choosing Φ to be the identity function. To avoid this we need to encourage Φ to be selective. We achieve this by imposing a representational bottleneck, restricting $\Phi(\mathbf{x}) \in \{1, \dots, C\}$ to a space of C discrete classes, and consequently imposing a ceiling on the entropy of $\Phi(\mathbf{x})$ of $\ln C$. Using an explicit bottleneck is a simple approach that has the added benefit of letting us directly learn a classification function.

3.1.1 Soft clusters

In practice, rather than learning a deterministic clustering map, we consider neural networks $\bar{\Phi}(\mathbf{x}) \in \mathbb{R}_+^C$ that terminate in a softmax layer, so we can interpret $z \sim \bar{\Phi}(\mathbf{x})$ as generating labels with probability $P(z = c|\mathbf{x}) = \bar{\Phi}_c(\mathbf{x})$. Let $z \sim \bar{\Phi}(\mathbf{x})$ and $z' \sim \bar{\Phi}(\mathbf{y})$, and introduce a control parameter λ . We can then rewrite Eq. (1) as:

$$\max_{\bar{\Phi}} I_{\lambda}(\bar{\Phi}(\mathbf{x}), \bar{\Phi}(\mathbf{y})), \quad (2)$$

where information is given by:

$$I_{\lambda}(z, z') = \sum_{c, c'=1}^C P(z = c, z' = c') \cdot \ln \frac{P(z = c, z' = c')}{P(z = c)^{\lambda} \cdot P(z' = c')^{\lambda}}. \quad (3)$$

Given a dataset $(\mathbf{x}_1, \mathbf{y}_1), \dots, (\mathbf{x}_n, \mathbf{y}_n)$ of example image pairs and letting \mathbf{e}_c be the one-hot c -th coordinate vector, the probabilities in Eq. (3) can be written compactly, and approximated from image batches instead of the entire dataset, as follows:

$$P(z = c) = P(z' = c) = \mathbf{e}_c^{\top} \frac{1}{n} \sum_{i=1}^n \bar{\Phi}(\mathbf{x}_i), \quad (4)$$

$$P(z = c, z' = c') = \mathbf{e}_c^{\top} \left(\frac{1}{n} \sum_{i=1}^n \bar{\Phi}(\mathbf{x}_i) \bar{\Phi}(\mathbf{y}_i)^{\top} \right) \mathbf{e}_{c'}. \quad (5)$$

With $\lambda = 1$, Eq. (3) is simply the KL-divergence between the joint probability (in the numerator) and the product of marginals (in the denominator). As such, maximizing Eq. (3) will make these two probabilities as *different* as possible, resulting in random variables that are more dependent (illustrated in Fig. 2).

3.1.2 Inherent cluster mass equalization and alternative formulations

We now show that Eq. (1) includes an inherent cluster mass equalisation bias which actively avoids the trivial solution of predicting the same cluster for all inputs. This can be easily seen by considering the

degenerate case where $\mathbf{x} = \mathbf{y}$ so that the common part between two observations, which information is used to distill, is trivially their entirety. Due to the fact that $\Phi(\mathbf{x})$ is a deterministic function of \mathbf{x} , $I(\Phi(\mathbf{x}), \Phi(\mathbf{x})) = H(\Phi(\mathbf{x})) - H(\Phi(\mathbf{x})|\Phi(\mathbf{x})) = H(\Phi(\mathbf{x}))$ so that Eq. (1) reduces to $\max_{\Phi} H(\Phi(\mathbf{x}))$, where H denotes entropy. Thus the best Φ partitions the mass of the data equally among the C clusters. The same result is found if soft clustering is used instead.¹ This further suggests that formulation (1) can produce meaningful clusters regardless of the amount of difference between images \mathbf{x} and \mathbf{y} (which will become relevant when \mathbf{x} and \mathbf{y} are neighbouring patches extracted from the same image, as we shall see). Note that while the formulation does not collapse if $\mathbf{x} = \mathbf{y}$, as with the case if we had chosen $\max_{\Phi} I(\mathbf{x}, \Phi(\mathbf{x})) = \max_{\Phi} H(\Phi(\mathbf{x}))$, it is no longer possible to exploit *differences* between \mathbf{x} and \mathbf{y} to identify a more abstract common representation.

3.1.3 λ -controllable cluster mass equalization

Using our λ -adapted version of the mutual information formula, we can explicitly control the balance of clusters produced by Φ . To understand the effect of λ , note from Eq. (3) that $I_{\lambda}(z, z') = I_1(z, z') + (\lambda - 1) \cdot (H(z) + H(z'))$, so setting $\lambda > 1$ forces Φ to produce a more evenly spread clustering and $\lambda < 1$ produces a more uneven clustering (Fig. 7). High λ can be used to overcome poor initialisation and heavily biased initial cluster assignments, or equivalently to force the network to use its full expressive capacity, particularly when the number of output channels is large. This marks an improvement over many of the methods discussed in Section 2 that depend heavily on the initial clustering produced by Φ , and gives ID a degree of robustness to the choice of underlying network architecture.

Furthermore, in a true unsupervised setting the number of ground truth clusters is not known. ID is naturally able to deal with this as the conditional entropy portion of mutual information shrinks unnecessary modes in the clustering, as long as λ is not too high. Thus ID only requires the user to specify an *upper limit* on the number of output clusters (i.e. number of channels in the network output). ID actually outperforms when the number of output clusters is greater than the ground truth as the network becomes more expressive².

3.2 Image clustering

We now apply ID to transform invariance, resulting in *Invariant* ID (IID) for image clustering. The key idea is in a fully unlabelled and unstructured dataset we are not privy to which images are observations of the same phenomenon (used for Eq. (2)). However we can generate \mathbf{y} from \mathbf{x} by applying random transformations g . In an image understanding context, g would be geometric warps such as scaling and rotation or colour warps such as changes in contrast and saturation. We assume that none of these effects should change the content of the image, so that $\Phi(g\mathbf{x}) = \Phi(\mathbf{x})$. This could be incorporated as a constraint in any clustering method; however in most implementations one would translate this into an additional term in the objective function, requiring a new weight parameter. Our intuition is that a similar effect can be obtained in a much simpler way by substituting $\mathbf{y} = g\mathbf{x}$ in Eq. (2), which results in the objective function:

$$\max_{\Phi} I_{\lambda}(\Phi(\mathbf{x}), \Phi(g\mathbf{x})). \quad (6)$$

Intuitively this means the class associated to an image and its deformed versions should be maximally informative. In practice, this is obtained when the classes are the same. Eq. (6) can be directly minimized over batches of images \mathbf{x} and their deformed versions $g\mathbf{x}$, to train a model Φ that performs image clustering. Section 4.2 describes STL experiments for this simple setting.

¹In this case $H(\bar{\Phi}(\mathbf{x})|\bar{\Phi}(\mathbf{x}))$ is not necessarily zero due to the non-determinism of $\bar{\Phi}(\mathbf{x})$. However, this quantity must eventually become zero to maximize the information $H(\bar{\Phi}(\mathbf{x})) - H(\bar{\Phi}(\mathbf{x})|\bar{\Phi}(\mathbf{x}))$. In other words, $\bar{\Phi}(\mathbf{x})$ reduces to a deterministic function of the data; the softmax output automatically has a single high value.

²Note that our method does not fundamentally rely on setting $\lambda \neq 1$ or an excessive number of output channels, and still outperforms the state-of-the-art without either.

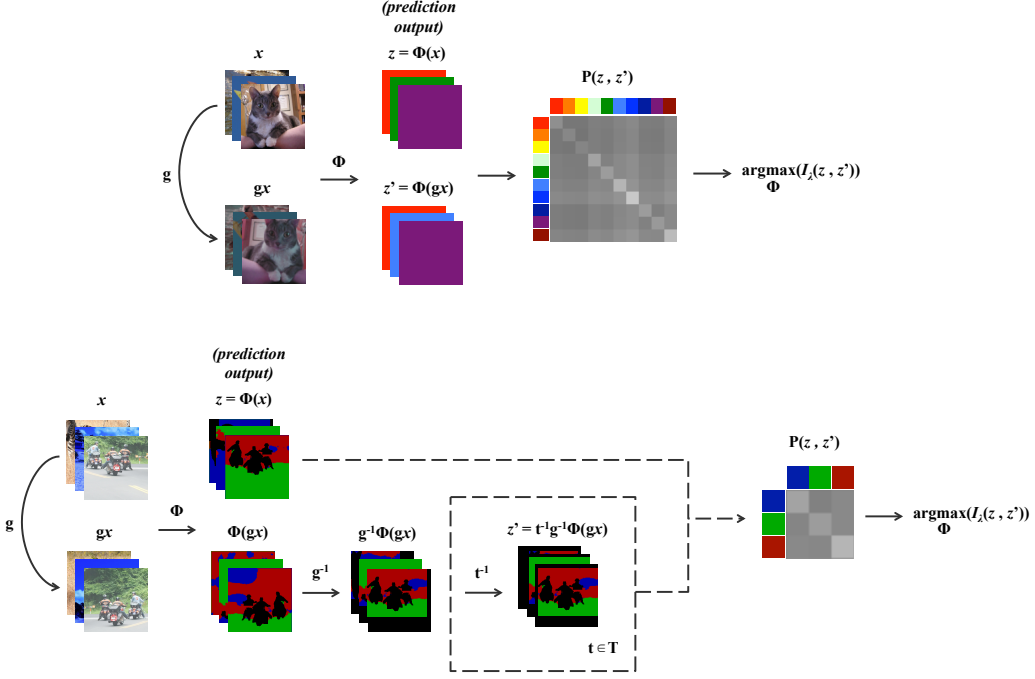


Figure 3: Top: IID for image clustering. Bottom: IID for image segmentation. Dashed line denotes operation implemented as convolution. I_{λ} denotes mutual information formula (Eq. (3)).

3.3 Image segmentation

We now apply IID to clustering patches for image segmentation, again by combining information distillation with transform invariance. First we examine the special case of when the transform is a small shift, before proceeding to the general formulation for multiple composed transforms.

3.3.1 Distillation from neighbouring patches

For segmentation, distillation operates not on pairs of whole images but pairs of image patches. We would like to apply Eq. (2) to a large number of *patch pairs* where each pair constitutes observations of the same visual phenomenon, and as before we have no label information about each patch. Let image $\mathbf{x} \in \mathbb{R}^{H \times W \times 3}$ be a tensor, $u \in \Omega = \{1, \dots, H\} \times \{1, \dots, W\}$ a pixel location, and \mathbf{x}_u a patch centered at u . We can generate such pairs by considering nearby patches, i.e. $(\mathbf{x}_u, \mathbf{x}_{u+t})$ from sampling random locations $\{u\}$ and their small displacements by some $t \in T \subset \mathbb{Z}^2$. Additionally, instead of explicitly cropping and computing the representation $\Phi(\mathbf{x}_u) \in \mathbb{R}^C$ for each individual patch, all of these can be computed in parallel by a single application $\Phi(\mathbf{x}) \in \mathbb{R}^{H \times W \times C}$ of the convolutional network to the full image \mathbf{x} . Then the representation of patch \mathbf{x}_u can be recovered as column u of the resulting tensor, namely $\Phi(\mathbf{x}_u) = \Phi_u(\mathbf{x})$. Likewise, all patch pairs can be formed efficiently by shifting the whole tensor $\Phi_u(\mathbf{x})$. In fact, since $\Phi(t^{-1}\mathbf{x}) = t^{-1}\Phi(\mathbf{x})$, the representation of patch $\mathbf{x}_{u+t} = (t^{-1}\mathbf{x})_u$ can be read from tensor $\Phi(\mathbf{x})$ at location $t^{-1}(u) = u - t$.

In this manner we can express maximising information (Eq. (6)) between two neighbouring patches, or maximising the informativeness of a patch's class for its neighbour's class, using the following objective:

$$I_{\lambda}^*(\Phi(\mathbf{x}), t^{-1}\Phi(\mathbf{x})), \quad (7)$$

where $*$ is used to indicate that information is computed as an expectation over pixels. This notation clarifies that the goal is to maximize the information between each patch label and neighbouring patch label, over the expectation of all patch centres. The underlying joint, Eq. (5), can be written as:

$$P(z, z') = \sum_{t \in T} P(z, z'|t) \cdot P(t) = \frac{1}{n|\Omega||T|} \sum_{i=1}^n \sum_{u \in \Omega} \sum_{t \in T} \bar{\Phi}_u(\mathbf{x}_i) \cdot \bar{\Phi}_{u+t}(\mathbf{x}_i)^{\top}, \quad (8)$$

which is the auto-correlation of tensor $\bar{\Phi}_u(\mathbf{x}_i)$. This is simply a standard co-occurrence probability estimation: for each pair of classes, to estimate $P(\text{class}(\mathbf{x}) = z, \text{class}(\mathbf{y}) = z'|t)$ from paired data (\mathbf{x}, \mathbf{y}) where \mathbf{y} is related to \mathbf{x} by spatial shift t , it counts the number of times \mathbf{x}_i is clustered as class z and \mathbf{y}_i is clustered as class z' .

Crucially, there is no need to sequentially perform the sums because Eq. (8) is exactly the equation for convolution. This means we can densely sample all possible displacements t for all pixels u and all batch images i in parallel (illustrated in Fig. 3).

3.3.2 Distillation from transformed patches in general

We can generalise Eq. (7) by incorporating image transformations (such as the warps already discussed in Section 3.2) other than small shifts. First, let $g : \mathbb{R}^{H \times W \times 3} \rightarrow \mathbb{R}^{H \times W \times 3}$ be a general smooth image warp (in practice the spatial domain is discretized by interpolation and padding as needed). Formally, g can operate on either the data of each patch \mathbf{x}_u (for example by flipping or colour distortion) or its location (moving it to a different location in the image). Therefore, in addition to predictions being locally consistent (Section 3.3.1), we would like to specify that the heatmap result is the same in the same location if no spatial change is applied (e.g. simply tinting the image should result in an identical heatmap) but varies *with* any spatial changes (e.g. shifting, rotating or flipping the entire image should result in the heatmap also being shifted, rotated or flipped)³. Thus while previously in Section 3.3.1 we were simply seeking locally translation invariant heatmaps, now we seek its generalisation: local translation invariance with non-spatial warp invariance and global spatial warp equivariance⁴.

Again, note we can use the convolutional nature of Φ to compute the heatmap for each transformed patch in parallel. If we rewrite the second argument of Eq. (7) to incorporate general transforms g (for simplicity we overload g so that when applied to coordinates it either reduces to its obvious $g : \mathbb{R}^2 \rightarrow \mathbb{R}^2$ form if g is a purely spatial image warp, else is the identity for e.g. colour distortion) we obtain:

$$\Phi((g\mathbf{x})_{g(u)+t}) = \Phi_{g(u)+t}(g\mathbf{x}) = [t^{-1}g^{-1}\Phi]_u(g\mathbf{x}). \quad (9)$$

Let us consider how this achieves our desired heatmap properties, looking at the third term and its use in Eq. (7) in detail. In the case where g is a spatial warp, image \mathbf{x} is first warped by g , then the dense pixel labels $\Phi(g\mathbf{x})$ are computed, and finally the latter are warped back to their original positions, $g^{-1}\Phi(g\mathbf{x})$, before being correlated with $\Phi(\mathbf{x})$ (t^{-1} notwithstanding). To a first approximation, after spatial transformation g is compensated for, one can expect the pixel labels to be the same as for the original image (i.e. $\Phi(\mathbf{x}) \approx g^{-1}\Phi(g\mathbf{x})$), giving global spatial warp equivariance. Non-spatial warp invariance is achieved because when g is not a spatial warp, applying g to a patch at location u changes its content but g^{-1} is taken to be the identity (e.g. the result for colour jittered patch is paired with the result for its non-jittered original, t^{-1} notwithstanding). Local spatial translation invariance is given since the reversal of small shift t^{-1} is not present.

We can write this in a simpler form by functionally composing t^{-1} and g^{-1} . Since $g^{-1} = \mathbb{1}$ in the case of invariance to non-spatial warps, which is not strictly an inverse of g , we replace it with the general reciprocal g^* . Let g be the composition of several warping functions and g^* be the composition of several reciprocals, i.e. $g = g_m \circ \dots \circ g_1$ and $g^* = g_1^* \circ \dots \circ g_m^*$, and let t^{-1} be incorporated by setting $g_1 = \mathbb{1}$ and $g_1^* = t^{-1}$. We obtain the canonical objective for image segmentation:

$$\max_{\Phi} I_{\lambda}^*(\Phi(\mathbf{x}), g^*\Phi(g\mathbf{x})). \quad (10)$$

³Fully convolutional networks may appear to give this for free in the case of translation, but in practice this is not always the case as images are truncated by shifting.

⁴At the patch level these are all cases of encouraging patches that we know to match up through the image transform to have the same label, and therefore equivariance at the heatmap scale is expressible as invariance at the patch level. This explains our method name *Invariant Information Distillation*.

3.4 Relating information distillation to other clustering methods

3.4.1 Information bottleneck

An alternative approach is to constrain the representation using an *information bottleneck*. The multivariate information bottleneck (MIB) Friedman et al. [2001], Wang et al. [2010] version of Eq. (1) is:

$$\min_{\Phi} I(\mathbf{x}, \Phi(\mathbf{x})) + I(\mathbf{y}, \Phi(\mathbf{y})), \quad \text{subject to } I(\mathbf{x}, \mathbf{y}) = I(\Phi(\mathbf{x}), \Phi(\mathbf{y})). \quad (11)$$

Since Φ is a deterministic function of the data, $I(\mathbf{x}, \Phi(\mathbf{x})) = H(\Phi(\mathbf{x}))$ is simply the entropy of the representation. Hence, MIB seeks for the most compact representation that preserves all (in practice, most of) the mutual information between \mathbf{x} and \mathbf{y} . In our case, the representation entropy is bounded by $\ln C$ and we approach $I(\mathbf{x}, \mathbf{y}) = I(\Phi(\mathbf{x}), \Phi(\mathbf{y}))$ by maximizing the equation’s right hand side.

3.4.2 Generative clustering

If $\mathbf{x}' = f(\mathbf{x})$ is an invertible transformation of the data space, we see that the solution to Eq. (1) does not change as long as the function Φ is powerful enough to compute f^{-1} . This is a property shared by information-based criteria since information itself is invariant to invertible data transformations (i.e. $I(\mathbf{x}, \mathbf{y}) = I(f(\mathbf{x}), f(\mathbf{y}))$).

The latter is very different from generative clustering techniques such as k-means and probabilistic k-means (and, by extension, to generative methods in general), which are very sensitive to distortions of the data. Formally, generative methods fit probability distributions $p(\mathbf{x}|c)$ to the data in each cluster c , minimizing the negative log likelihood $E_{\hat{p}(\mathbf{x}|c)}[-\log p(\mathbf{x}|c)]$ where $\hat{p}(\mathbf{x}|c)$ is the empirical distribution of the cluster. The latter quantity is the same as the cross entropy $H(\hat{p}(\cdot|c), p(\cdot|c))$, which, in some cases such as Gaussian probabilistic k-means, further simplifies in an approximation of the (Gaussian) entropy $H(\mathbf{x}|c)$ of a cluster.

Thus generative modeling tries to minimize the entropy of the data (subject to some modeling approximation), a quantity which is not invariant to data transformations. Information distillation, bottleneck, and co-clustering, on the other hand, look for clusters that most effectively identify different data points, which corresponds to equi-partitioning and is invariant to transformations. The latter is a mixed blessing as data often comes in spaces whose metric is at least somewhat informative. Generative clustering can exploit this (i.e. if \mathbf{x} and \mathbf{y} are close as vectors, they should cluster together), whereas information distillation cannot, at least in principle. However, in practice the learned representation function Φ is smooth, implicitly providing a degree of metric sensitivity.

4 Experiments

IID is particularly suited to segmentation due its dense convolutional formulation and use of spatial proximity as a learning signal in this case. A few baselines also utilise spatial context (Doersch et al. [2015], Isola et al. [2015]) but none are formulated efficiently for dense prediction (i.e. without sampling pixels in the heatmap for the loss). IID’s end-to-end formulation and implicit cluster mass equalisation (since maximising mutual information implies maximising class entropy, see Section 3.1.3) benefit both segmentation and image clustering.

4.1 Image segmentation

Datasets. COCO-Stuff-15 (Caesar et al. [2016]) contains 15 texture classes, such as sky, building, food and furniture; COCO-Stuff-3 is a subset containing the sky, plants and ground classes. Object (non-“Stuff”) pixels are ignored using binary masks; images where less than 25% of the pixels belong to the categories of interest are also ignored. Potsdam (ISPRS) contains 24 6000×6000 pixel aerial RGB photographs; we partition these into 5000 training and 400 testing non-overlapping 400×400 images. Potsdam-6 contains the 6 classes of roads, cars, low vegetation, trees, buildings and clutter; Potsdam-3 contains 3 classes formed from merging adjacent pairs of classes from Potsdam-6. Training and test set sizes are reported in Table 3.

Dataset Metric	COCO-Stuff-3			COCO-Stuff-15			Potsdam-3			Potsdam-6		
	ACC	NMI	ARI	ACC	NMI	ARI	ACC	NMI	ARI	ACC	NMI	ARI
IID, $\lambda = 1$	0.704	0.313	0.348	0.337	0.140	0.083	0.525	0.141	0.139	0.509	0.209	0.158
IID, $\lambda = 1.5$	0.699	0.323	0.336	0.336	0.137	0.084	0.639	0.240	0.267	0.523	0.227	0.175
IID+, $\lambda = 1$	0.711	0.277	0.292	0.357	0.133	0.070	0.725	0.274	0.261	0.578	0.220	0.150
DAC	0.428	0.008	0.013	0.233	0.037	0.018	0.404	0.011	0.009	0.328	0.032	0.016
DAC+	0.493	0.060	0.087	0.226	0.031	0.018	0.431	0.024	0.025	0.362	0.037	0.027
CON*	0.618	0.214	0.155	0.303	0.057	0.037	0.491	0.092	0.048	0.385	0.081	0.031
DEC*	0.616	0.180	0.176	0.301	0.066	0.033	0.555	0.098	0.104	0.409	0.081	0.052
Doersch*	0.466	0.060	0.035	0.294	0.042	0.027	0.413	0.044	0.035	0.333	0.049	0.022
Dosovitskiy*	0.548	0.089	0.098	0.334	0.063	0.028	0.501	0.048	0.056	0.379	0.070	0.045
SIFT*	0.459	0.027	0.026	0.239	0.039	0.035	0.365	0.001	0.002	0.301	0.006	0.006
Random CNN*	0.419	0.024	0.004	0.248	0.040	0.008	0.413	0.024	0.004	0.339	0.026	0.015
Random CNN	0.411	0.011	0.005	0.208	0.019	0.008	0.398	0.016	0.012	0.344	0.029	0.025

Table 1: Segmentation results. ACC is per-pixel accuracy, dataset- n indicates n ground truth clusters, (+) indicates a number of output clusters greater than the ground truth, (*) indicates use of k-means.

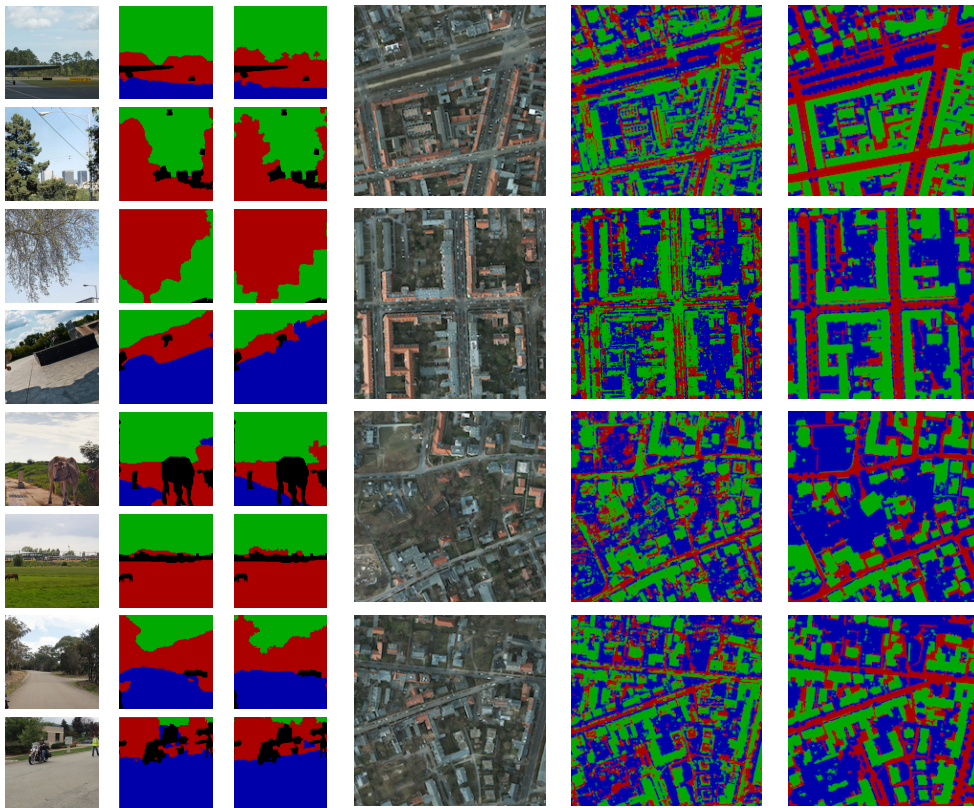


Figure 4: Qualitative results on COCO-Stuff-3 and Potsdam-3. Left to right for each triplet: input image, IID predictions ($\lambda = 1$), ground truth.

Architecture. Inspired by DeepLab (Chen et al. [2016]), we use a fully-convolutional adaptation of VGG11 (Simonyan and Zisserman [2014]). Bilinear upsampling is used to ensure input and output sizes are identical. All experiments use the same architecture, randomly initialised.

Training. IID experiments do not use separate data augmentation, relying solely on the transformations in Eq. (10). Batch size is 40 image pairs, learning rate is 10^{-5} . The sampled transformations used are horizontal flips, large shifts (between 40 and 100 pixels), and additive colour changes in HSV space (up to 15%). We maximize mutual information according to Eq. (10), using probabilities computed efficiently by convolution within a neighbourhood of 21×21 pixels for the dense small shift transformations T (see Eq. (8) and Fig. 3).

Evaluation. We compare against Chang et al. [2017] (DAC), Isola et al. [2015] (Co-Occurrence Network or CON), Xie et al. [2016] (DEC), Doersch et al. [2015], Dosovitskiy et al. [2016], Lowe [2004] (SIFT), and randomly initialised networks. Baselines were adapted for the task of segmentation by running k-means on extracted feature vectors. We avoided pre-training (DEC), auxiliary losses not reported in publication (DAC), and ensured metrics were evaluated on a test set that was held-out and unseen during training for all experiments. All methods operate on raw images. We evaluate using per-pixel accuracy (ACC) and clustering metrics NMI and ARI.

Results. All variants of IID achieve higher accuracy than the baselines on unseen test data, for all 4 datasets (Table 1), outperforming the state-of-the-art by approximately 10-20%. Notably, there is a striking level of fine grained detail in the produced outputs (Fig. 4). Higher λ has a positive effect, by constraining the classes to have more equal size (Fig. 7). IID performs particularly well on datasets with fewer classes (COCO-Stuff-3, Potsdam-3). This is expected behaviour as the method is provided with no semantic grounding, and therefore unsurprisingly prefers to combine rather than separate e.g. “trees” and “low vegetation” in satellite images. Similarly, in COCO-Stuff-15, grass playing fields are considered as “ground” and vegetables as “food”, rather than both being placed in “plants” with grass, leaves and trees. Such semantically distinct classes are difficult to distinguish from just visual appearance (even for humans), and this constitutes the main challenge for our method.

Our results suggest that end-to-end learning, where the clustering happens within the network model, works better than an external k-means (even if the centroids are learned, as in DEC). Unlike DAC, our end-to-end procedure does not alternate between estimating cluster centers and assigning samples to them, making it less dependent on initialisation, which may explain its better performance.

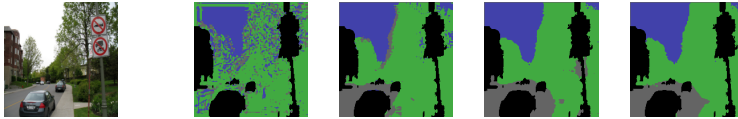


Figure 5: IID automatically discovering sky, vegetation and roads in successive epochs.

For unlabeled data the true number of clusters may not be known a-priori. We test this case by overestimating the true number of clusters ($3\times$ more for Potsdam, and 15 and 20 clusters for COCO-Stuff-3 and 15, respectively). These variants are denoted with a plus (+) (Table 1). Both IID and DAC perform as well under these conditions, in some cases even more so (since the network is more expressive and outlier or low-confidence samples can be placed in new clusters), though IID still outperforms DAC.

4.2 Image clustering

	IID	DAC	DEC*	Dosovitskiy*	SIFT*	Random CNN*	Random CNN
ACC	0.338	0.222	0.263	0.323	0.264	0.246	0.134
NMI	0.276	0.116	0.142	0.223	0.227	0.138	0.030
ARI	0.163	0.059	0.082	0.131	0.106	0.076	0.006

Table 2: Results on unlabelled STL-10. ACC is classification accuracy, (*) indicates use of k-means.

Datasets. All experiments use the unlabelled 100k partition of STL-10 (Coates et al. [2011]) for training, and the labelled 8k test partition for testing. The latter contains 10 object classes ranging from cats to trucks.

Architecture. We use a simple network containing 4 convolutional layers (with a maximum of 512 features) separated by 3 max-pooling layers and followed by a single linear classification layer.

Training. Batch size is 400 image pairs, learning rate is 10^{-4} . The sampled transformations used are horizontal flips, crops, rescales, and additive colour changes in HSV space (up to 40%). Mutual information is maximised according to Eq. (6).

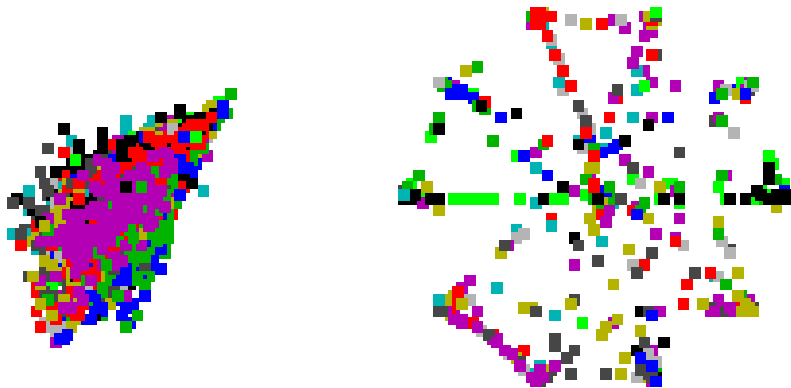
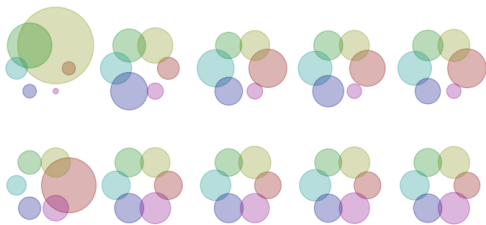


Figure 6: Left to right: before and after projected predictions of network trained with IID on STL-10.

Evaluation. We compare against Chang et al. [2017] (DAC), Xie et al. [2016] (DEC), Dosovitskiy et al. [2016], Lowe [2004] (SIFT), and randomly initialised networks. Where required, k-means was run on baseline feature vectors. As before, we avoided pre-training (DEC), auxiliary losses not reported in publication (DAC), and ensured metrics were evaluated on a test set that was held-out and unseen during training for all experiments.

Results. We outperform all baselines by at least 7% except Dosovitskiy et al. [2016], which we outperform by 1.5%. This is unsurprising since the objectives are both forms of increasing the correlation between predictions of images processed through image transformations. The major practical difference is IID is easily scalable whereas Dosovitskiy is not; the batch sizes we could run were 400 for the former (800 images in total) and a maximum of 80 for the latter (since we used 10 exemplars per image, which is already a reduction compared to the original work). This meant training was approximately $5\times$ slower for Dosovitskiy (see Section 2 for additional discussion).



Dataset	COCO-Stuff		Potsdam	
Classes	3	15	3	6
Train.	16000	30000	5000	5000
Val.	2000	2000	400	400

Figure 7: IID+ cluster masses on Potsdam-3, first 5 epochs, with $\lambda = 1$ (top) and $\lambda = 1.5$ (bottom).

Table 3: Number of images in each subset used in the segmentation experiments.

4.3 Unsupervised clustering compared to representation learning

The main goal of our method is pure unsupervised clustering, not merely feature learning, and not as pre-training for supervised regimes. There is intrinsic scientific interest in the problem of discovering classes in raw unlabelled data, which is why methods such as k-means or spectral clustering were created. In practice there are many cases where labelled data is not available, due to resource constraints or lack of human knowledge; nevertheless, we recognize that the transferability of features to the supervised case is useful. Our experiments showed that features learned for STL-10 using IID achieve 77.7% classification accuracy, which beats the best supervised result among our baselines (Dosovitskiy et al. [2016] at 74.2%).

5 Conclusions

In this work we show that meaningful deep representations can be extracted from images by simply maximizing the mutual information between the representations of adjacent or distorted patches. We show that this is a viable approach for fully unsupervised image segmentation and image clustering into semantic classes, beating state-of-the-art baselines in both cases. Our proposal opens up new interesting research directions, such as learning more complex class hierarchies with mutual information, and optimizing information in videos over time.

References

- Pulkit Agrawal, Joao Carreira, and Jitendra Malik. Learning to see by moving. In *Computer Vision (ICCV), 2015 IEEE International Conference on*, pages 37–45. IEEE, 2015.
- Suzanna Becker and Geoffrey E Hinton. Self-organizing neural network that discovers surfaces in random-dot stereograms. *Nature*, 355(6356):161, 1992.
- Holger Caesar, Jasper Uijlings, and Vittorio Ferrari. Coco-stuff: Thing and stuff classes in context. *arXiv preprint arXiv:1612.03716*, 2016.
- Jianlong Chang, Lingfeng Wang, Gaofeng Meng, Shiming Xiang, and Chunhong Pan. Deep adaptive image clustering. In *Proceedings of the IEEE Conference on Computer Vision and Pattern Recognition*, pages 5879–5887, 2017.
- Liang-Chieh Chen, George Papandreou, Iasonas Kokkinos, Kevin Murphy, and Alan L Yuille. Deeplab: Semantic image segmentation with deep convolutional nets, atrous convolution, and fully connected crfs. *arXiv preprint arXiv:1606.00915*, 2016.
- Adam Coates, Andrew Ng, and Honglak Lee. An analysis of single-layer networks in unsupervised feature learning. In *Proceedings of the fourteenth international conference on artificial intelligence and statistics*, pages 215–223, 2011.
- Thomas M Cover and Joy A Thomas. *Elements of information theory*. John Wiley & Sons, 2012.
- Rodrigo Santa Cruz, Basura Fernando, Anoop Cherian, and Stephen Gould. Deeppermnet: Visual permutation learning. *arXiv preprint arXiv:1704.02729*, 2017.
- Jifeng Dai, Kaiming He, and Jian Sun. Boxsup: Exploiting bounding boxes to supervise convolutional networks for semantic segmentation. In *Proceedings of the IEEE International Conference on Computer Vision*, pages 1635–1643, 2015.
- Carl Doersch, Abhinav Gupta, and Alexei A Efros. Unsupervised visual representation learning by context prediction. In *Proceedings of the IEEE International Conference on Computer Vision*, pages 1422–1430, 2015.
- Alexey Dosovitskiy, Philipp Fischer, Jost Tobias Springenberg, Martin Riedmiller, and Thomas Brox. Discriminative unsupervised feature learning with exemplar convolutional neural networks. *IEEE transactions on pattern analysis and machine intelligence*, 38(9):1734–1747, 2016.
- Nir Friedman, Ori Mosenzon, Noam Slonim, and Naftali Tishby. Multivariate information bottleneck. In *Proceedings of the Seventeenth conference on Uncertainty in artificial intelligence*, pages 152–161. Morgan Kaufmann Publishers Inc., 2001.
- Ross Girshick, Jeff Donahue, Trevor Darrell, and Jitendra Malik. Rich feature hierarchies for accurate object detection and semantic segmentation. In *Proceedings of the IEEE conference on computer vision and pattern recognition*, pages 580–587, 2014.
- Klaus Greff, Rupesh Kumar Srivastava, and Jürgen Schmidhuber. Binding via reconstruction clustering. *arXiv preprint arXiv:1511.06418*, 2015.
- Klaus Greff, Antti Rasmus, Mathias Berglund, Tele Hao, Harri Valpola, and Juergen Schmidhuber. Tagger: Deep unsupervised perceptual grouping. In *Advances in Neural Information Processing Systems*, pages 4484–4492, 2016.

- J. A. Hartigan. Direct clustering of a data matrix. In *Journal of the American Statistical Association*, 1972.
- Ronghang Hu, Piotr Dollár, Kaiming He, Trevor Darrell, and Ross Girshick. Learning to segment every thing. *arXiv preprint arXiv:1711.10370*, 2017.
- Phillip Isola, Daniel Zoran, Dilip Krishnan, and Edward H Adelson. Learning visual groups from co-occurrences in space and time. *arXiv preprint arXiv:1511.06811*, 2015.
- ISPRS. ISPRS 2D Semantic Labeling Contest. <http://www2.isprs.org/commissions/comm3/wg4/semantic-labeling.html>. [Online; accessed 10-March-2018].
- Hsin-Ying Lee, Jia-Bin Huang, Maneesh Singh, and Ming-Hsuan Yang. Unsupervised representation learning by sorting sequences. In *2017 IEEE International Conference on Computer Vision (ICCV)*, pages 667–676. IEEE, 2017.
- Jonathan Long, Evan Shelhamer, and Trevor Darrell. Fully convolutional networks for semantic segmentation. In *Proceedings of the IEEE conference on computer vision and pattern recognition*, pages 3431–3440, 2015.
- David G Lowe. Distinctive image features from scale-invariant keypoints. *International journal of computer vision*, 60(2):91–110, 2004.
- Mehdi Noroozi and Paolo Favaro. Unsupervised learning of visual representations by solving jigsaw puzzles. In *European Conference on Computer Vision*, pages 69–84. Springer, 2016.
- George Papandreou, Liang-Chieh Chen, Kevin P Murphy, and Alan L Yuille. Weakly-and semi-supervised learning of a deep convolutional network for semantic image segmentation. In *Proceedings of the IEEE international conference on computer vision*, pages 1742–1750, 2015.
- Deepak Pathak, Philipp Krahenbuhl, and Trevor Darrell. Constrained convolutional neural networks for weakly supervised segmentation. In *Proceedings of the IEEE international conference on computer vision*, pages 1796–1804, 2015.
- Deepak Pathak, Philipp Krahenbuhl, Jeff Donahue, Trevor Darrell, and Alexei A Efros. Context encoders: Feature learning by inpainting. In *Proceedings of the IEEE Conference on Computer Vision and Pattern Recognition*, pages 2536–2544, 2016.
- Karen Simonyan and Andrew Zisserman. Very deep convolutional networks for large-scale image recognition. *arXiv preprint arXiv:1409.1556*, 2014.
- Pascal Vincent, Hugo Larochelle, Isabelle Lajoie, Yoshua Bengio, and Pierre-Antoine Manzagol. Stacked denoising autoencoders: Learning useful representations in a deep network with a local denoising criterion. *Journal of Machine Learning Research*, 11(Dec):3371–3408, 2010.
- C. Wang, C. Domeniconi, and K. B. Laskey. Information bottleneck co-clustering. In *Proc. IBCC TMW*, 2010.
- Junyuan Xie, Ross Girshick, and Ali Farhadi. Unsupervised deep embedding for clustering analysis. In *International conference on machine learning*, pages 478–487, 2016.
- Jianwei Yang, Devi Parikh, and Dhruv Batra. Joint unsupervised learning of deep representations and image clusters. In *Proceedings of the IEEE Conference on Computer Vision and Pattern Recognition*, pages 5147–5156, 2016.